Clays and Clay Minerals, Vol. 50, No. 2, 186–197, 2002.

LEPIDOCROCITE IN HYDROTHERMAL SEDIMENTS OF THE ATLANTIS II AND THETIS DEEPS, RED SEA

NURIT TAITEL GOLDMAN[1,2], CHRISTIAN BENDER KOCH[3] AND ARIEH SINGER[2]

[1] The Open University of Israel, P.O. Box 39328 Tel Aviv, Israel
[2] The Seagram Center for Soil and Water Sciences, Faculty of Agricultural, Food and Environmental Quality Sciences, The Hebrew University of Jerusalem, Rehovot, Israel
[3] Chemistry Department, The Royal Veterinary and Agricultural University, Thorvaldsensvej 40, Frederiksberg, DK-1871 Frb.C., Denmark

Abstract—Lepidocrocite (γ-FeOOH) formation in the hydrothermal brines of the Thetis and Atlantis II Deeps in the Red Sea results in markedly different crystals (size and shape). The only foreign element associated with the crystals is Si and analyses of samples from the two deeps yielded average Si/Fe (molar) ratios of 0.03 and 0.11, respectively. The Si/Fe ratio does not affect formation of a perfect lattice along [010]. Direct observations of crystal morphology as well as X-ray diffraction patterns, Mössbauer and infrared spectra, all indicate that the Atlantis II Deep lepidocrocite is less crystalline than the Thetis Deep lepidocrocite. In one sample a poly-disperse size distribution was resolved indicating a fine-scale variation in precipitation conditions. Infrared spectroscopy suggests that the Si is adsorbed on the lepidocrocite surfaces, probably also forming polymers, as both Fe–O–Si and Si–O–Si bonds can be detected. The formation of the Atlantis II Deep lepidocrocite is due to fast oxidation of Fe^{2+}. The blanket-like layer of lepidocrocite in Atlantis II and Thetis Deeps lepidocrocite was probably formed as a result of precipitation during an abrupt oxidation event of the brine, triggered by down-welling of a condensed oxidized brine, which originated in the northern part of the Red Sea. A difference in Si concentrations determined the different crystal properties of the lepidocrocite formed in the two deeps.

Key Words—Analytical High-resolution Transmission Electron Microscopy, Atlantis II Deep, Electron Diffraction, Hydrothermal Sediments, Infrared Spectroscopy, Mössbauer Spectroscopy, Si associated with Lepidocrocite, Thetis Deep.

INTRODUCTION

Lepidocrocite (γ-FeOOH) in marine sediments influenced by hydrothermal brines has been reported from the Atlantis II Deep (A2D) and the Thetis Deep (TD), in the Red Sea. The A2D has been a continuously active hydrothermal site since its formation some 28000 years ago (Danielsson *et al.*, 1980). Hydrothermal fluids, which are leaching the Miocene evaporites and overlying sediments, have been trapped in the A2D forming submarine hot brine (Craig, 1969; Stoffers and Ross, 1972; Schoell and Faber, 1978; Dupré *et al.,* 1988). The metal cations in the venting water have created meter-thick deposits of oxides, silicates, carbonates and sulfides as the primary constituents. The sediments of the A2D have been investigated in several publications and include various Fe oxides and oxyhydroxides (Bischoff, 1969; Bäcker and Richter, 1973; Bignell, 1975; Butuzova *et al.,* 1990; Schwertmann *et al.,* 1998).

Bischoff (1969) first identified well-crystallized lepidocrocite in A2D. Lepidocrocite was detected mainly in two oxidized zones, the lowermost Detrital-Oxidic-Pyritic Zone (DOP) and the Central-Oxidic Zone (CO), but it also occurs as a few centimeters-thick layer towards the lower part of the uppermost Amorphous-Silicate Zone (AM), spreading over the whole of the Deep and forming a distinct marker horizon (LP) (Bäcker and Richter, 1973; Bignell, 1975; Butuzova *et al.,* 1990).

In the TD, lepidocrocite was reported by Bignell (1975), Butuzova and Lisitsyna (1984) and Scholten (1984) in Fe-rich layers together with magnetite and hematite. The presence of lepidocrocite in the northeast of the TD is related to hydrothermal activity which lasted till 1200 BP. Hydrothermal discharging fluids filled the northeast basin in the TD, causing the formation of a brine pool (simultaneously with the hydrothermal activity in the A2D) and subsequently precipitating Fe-facies types (Scholten *et al.,* 1991).

Lepidocrocite usually precipitates at fast oxidation of Fe^{2+} at ambient conditions with pH controlled between 5 and 7 (Cornell and Schwertmann, 1996). Iron oxides often retain the elements from the solution they formed in, either as substitutions or adsorbed and may therefore themselves reveal information on the geochemical conditions during formation. We therefore decided to undertake a structural and crystal chemistry investigation of the lepidocrocite from the Red Sea Deeps.

SAMPLES AND METHODS

Samples from the Red Sea Deeps had been collected by R.V. Valdivia in the 'Meseda 3' cruise for the Saudi-

* E-mail address of corresponding author: nuritg@oumail.openu.a c.il

Sudanese Red Sea Joint Commission for Exploration of Red Sea Resources. Three samples were chosen for the presentation based on their relatively high content of lepidocrocite (Table 1). The moist samples were stored at 4°C from the time of collection. Each sample was washed with distilled, deoxygenated water under a N_2 atmosphere in order to remove easily soluble salts. This procedure was used to prevent oxidation of Fe sulfides or Fe carbonates which are frequently found in the sediments of A2D. The samples were then freeze dried. The samples (GN072 and GN244) were suspended in alcohol and transferred to Cu-supported carbon or holey carbon films for transmission electron microscopy (TEM) analyses. Phase analyses and elemental analyses by energy dispersive X-ray (EDX) analysis were carried out either using a Jeol 20-10 HRTEM operated at 200 keV and equipped with an Oxford Instrument Link ISIS, or a Philips EM 430 operated at 300 keV equipped with an EDAX 9900. Counting time was 40–50 live seconds and the diameter of sampled area was 10 nm and 25 nm for samples GN072 and GN244, respectively. Calculated electron diffraction from high-resolution transmission electron micrographs (HRTEM) was obtained using Fast Fourier transformation in the 'Gatan' software.

The XRD analyses were carried out with a Philips 1050 powder diffractometer using CuKα radiation with a graphite curved monochromator in the diffracted beam, at a scanning step size of 0.02°2θ and a measuring time of 2 s per step. NBS640-silicon was added in ~10% weight as an internal standard. The fitting of the peaks profile was performed by using a Pseudo-Voigt function with APD computer program developed by Philips Export B.V. Phase identification was performed on the basis of ICDD card No. 44-1415 (lepidocrocite) and Card No. 29-713 (goethite). The unit-cell refinement was peformed by a least squares process (Celsiz). Rietveld simulation (Young DBWF 98 software) of the XRD patterns was used to quantify the lepidocrocite, goethite and siderite in the samples.

Mössbauer spectra were measured at temperatures between 5 and 298 K using a conventional constant acceleration spectrometer and a source of ^{57}Co in Rh. The spectrometer was calibrated using a foil of metallic Fe at room temperature, and isomer shifts are given relative to the centroid of this spectrum. Fittings of the spectra were performed using a least squares refinement with a combination of doublets and sextets of Lorentzian lineshape.

Infrared (IR) spectra were obtained using a Nicolet FTIR spectrometer. Absorbance and reflectance spectra were obtained for the A2D and TD samples after removing soluble salts. The spectra were recorded in the 4000–380 cm^{-1} range using the 'Omnic' software. Absorbance spectra were measured using 1000 mg of KBr and 10 mg of sample that were ground and pressed. A total of 66 scans per sample were collected for absorbance spectra. Reflectance spectra were measured using 30 mg samples, mixed and ground with KBr to make a total weight of 310 mg. Diffuse reflectance (DRIFT) spectra were measured by collecting 400 scans (Niemeyer *et al.,* 1992). The IR spectra were analyzed using the peak-fitting function in the 'Grams' software using Lorentzian lineshapes. Multiple points on either side of the region of interest were selected for linear baseline correction.

Three methods were used to characterize the chemical composition of the samples. The samples were treated with 0.2 M ammonium oxalate at pH 3 in the dark to extract highly reactive Fe oxides (Schwertmann, 1959, 1964; McKeague and Day, 1966) and with DCB (dithionite-citrate-bicarbonate) to dissolve all Fe oxides (Mehra and Jackson, 1960). The chemical composition of the solutions was determined using inductively coupled plasma atomic emission spectrometry (ICP-AES) and molar ratios were calculated assuming that the dissolved elements originated from the Fe oxides. These bulk ratios were compared with the results obtained by elemental analyses of individual particles (or clusters of a few particles), using the EDX spectrometers attached to the TEMs.

RESULTS AND DISCUSSION

X-ray diffraction

The XRD analysis revealed that lepidocrocite (GN072: 90 wt.%, GN076: 30 wt.%, GN244: 85 wt.%, respectively) and goethite are the main phases present; Mn-siderite (GN072 and GN076 <4 wt.%) and some clay were found as impurities (Figure 1) (Table 2). The content of the phases was estimated based on simulations of powder diffraction patterns for adequate mixtures using the Rietveld program.

Sample GN076 from A2D has the smallest lepidocrocite crystallites (10±2 nm) and its unit-cell parameters are: a = 1.253 nm±0.02; b = 0.3866 nm±0.007; and c = 0.3076 nm±0.009. In sample GN072, two profile functions of different breadth were needed (Figure 1a,b,c) for a

Table 1. Codes, positions, core depths and stratigraphic zones of the samples.

No.	Deep	Core	Positions	Location	Depth (m)	Zone
GN072	A2D	VA29-264 KS	21°21.44N, 38°04.032E	SW Passage	9.77	DOP2[1]
GN076	A2D	VA29-264 KS	21°21.44N, 38°04.032E	SW Passage	10.29	DOP2[1]
GN244	TD	VA29-728P	22°47.55N, 37°34.74E	NE Basin	1.70	Fe facies

[1] Detrital-oxidic pyritic Zone (Bäcker and Richter, 1973)

https://doi.org/10.1346/000986002760832784 Published online by Cambridge University Press

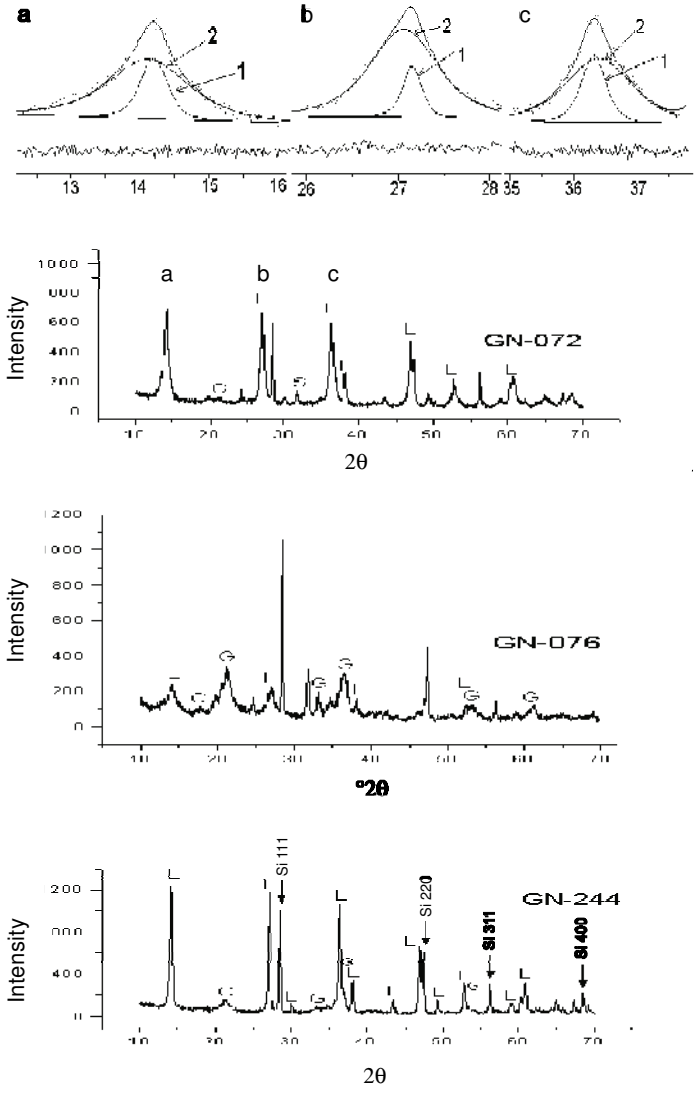

Figure 1. X-ray diffraction patterns of samples GN072, GN076 and GN244 with fitted (a) 200; (b) 210, and (c) 301 peaks from GN072 (L: lepidocrocite, G: goethite, S: siderite, Si: added Si standard).

good fit of peaks, indicating that two different crystallite sizes are present in the sample: a major part with sizes 15–20 nm (75–80%) and a minor part of larger crystallites 55–60 nm (20–25%). The unit-cell parameters of the finer fraction in this sample are a = 1.2534±0.0004 nm; b = 0.3871±0.001 nm; and c = 0.3070±0.001 nm. The coarser fraction has similar unit-cell parameters (within the uncertainty). The average calculated size of GN244 lepidocrocite is 55–60 nm and its unit-cell parameters are: a = 1.2526±0.002 nm; b = 0.3872±0.001 nm; and c = 0.3070±0.001 nm, *i.e.* similar to the other two samples. Thus no indication of lattice substitutions was obtained from the unit-cell parameters. None of the lepidocrocite samples contains maghemite or hematite as found in previous investigations.

Following the values of FWHM (full width at half maximum) of different peaks, the size of the crystallites in all samples in the [100] direction is smaller than any perpendicular directions, whereas the dimensions in the [010] and [001] directions are roughly equal. The ratio of the [100] to [010] (or [001]) directions is 0.6±0.1 and 0.4±0.1 for the lepidocrocite in samples GN072 and GN244, respectively.

Mössbauer spectroscopy

Lepidocrocite is paramagnetic at room temperature and antiferromagnetic below the Neel temperature (77 K) (Cornell and Schwertmann, 1996). Accordingly, the spectra measured at 295 K are dominated by quadrupole doublet splittings of

https://doi.org/10.1346/000986002760832784 Published online by Cambridge University Press

Table 2. X-ray diffraction data and crystallographic properties of lepidocrocite (Lep) from Atlantis II and Thetis Deeps.

GN072 N	°2θ	FWHM[1]	I/I_0	Lep. *hkl*	Other phases	GN076 N	°2θ	FWHM[1]	I/I_0	Lep. *hkl*	Other phases	GN244 N	°2θ	FWHM[1]	I/I_0	Lep. *hkl*	Other phases
1	14.02	1.02	100	200		1	14.05	1.45	57	200		1	14.08	0.39	100	200	
2	14.11	0.39	35	200*		2	17.73	0.6	6		Goethite	2	21.21	1.1	22		Goethite
3	19.72	0.72	6		Clays	3	19.64	0.48	13			3	27.05	0.28	75	210	
4	21.06	1.2	10		Goethite	4	20.40	0.64	7			4	29.98	0.4	4	101	
5	26.97	0.72	94	210		5	21.24	1.35	100		Goethite	5	33.15	0.75			Goethite
6	27.06	0.30	15	210*		6	24.59	0.22	6		Siderite	6	36.29	0.30	70	301	
7	29.98	0.37	5	101		7	26.95	1.02	47	210		7	36.84	0.45	16	410	Goethite
8	31.62	0.33	8		Siderite	8	31.79	0.27	25		Halite	8	38.07	0.22	15	111	
9	34.64	0.78	5		Goethite	9	33.21	0.81	20		Goethite	9	43.33	0.30	7	600, 311	
10	36.25	0.34	29	301*		10	34.67	0.57	15		Goethite	10	46.76	0.33	27	501	
11	36.33	0.98	89	301		11	36.19	1.26	73	301		11	46.91	0.25	22	020	
12	38.06	0.37	22	111		12	36.63	0.6	24		Goethite	12	49.23		7	220	
13	41.92	0.73	3		Siderite	13	38.10	0.33	10	111		13	52.71		19	511	
14	43.30	0.58	9	311, 600		14	39.98	0.58	5		Goethite	14	53.28				Goethite
15	45.87	0.47	3		Siderite	15	41.13	0.63	5		Goethite	15	56.76	0.50	1	121	
16	46.86	0.71	47	501		16	42.11	0.31	4		Siderite	16	58.93	0.37	6	800	
17	46.90	0.27	20	020		17	45.95	0.41	5		Halite	17	60.22	0.20	7	002	
18	49.25	0.40	9	220		18	47.00	0.7	23	020		18	60.70	0.30	20	321	
19	50.10	0.21	2		Goethite	19	50.50	0.34	2		Goethite	19	62.22	0.20	1	202	
20	52.68	0.94	30	511		20	52.34	0.4	6		Siderite	20	64.12	0.35	2	810	
21	52.76	0.31	2		Goethite	21	53.10	1.4	29		Goethite	21	64.88	0.32	9	711	
22	56.64	0.30	2	121		22	58.93	0.45	6	800		22	65.70	0.30	2	620	
23	58.94	0.62	7	800		23	60.69	0.8	10	321		23	67.22	0.26	7	212	
24	60.25	0.35	15	002		24	61.23	0.47	10		Goethite	24	68.36	0.26	11	521	
25	60.72	0.41	21	321		25	63.75	0.3	2		Goethite						
26	62.23	0.33	3	202		26	64.77	1.09	5	711							
27	64.82	1.02	17	711		27	67.10	1.3	7	212	Goethite						
28	65.82	0.56	2	620		28	68.58	0.96	5	521							
29	67.23	0.45	10	212													
30	68.36	0.67	17	521													
a = 1.2534 ± 0.0004 nm b = 0.3871 ± 0.001 nm c = 0.3070 ± 0.001 nm Two grain-size populations: 15–20 nm (75–80%) and 55–60 nm (20–25%)						a = 1.2534 ± 0.0002 nm b = 0.3871 ± 0.0007 nm c = 0.3076 ± 0.0009 nm average grain-size 10 ± 2 nm						a = 1.2526 ± 0.002 nm b = 0.3872 ± 0.001 nm c = 0.3070 ± 0.001 nm average grain size=55–60 nm					

[1] FWHM: full width at half maximum

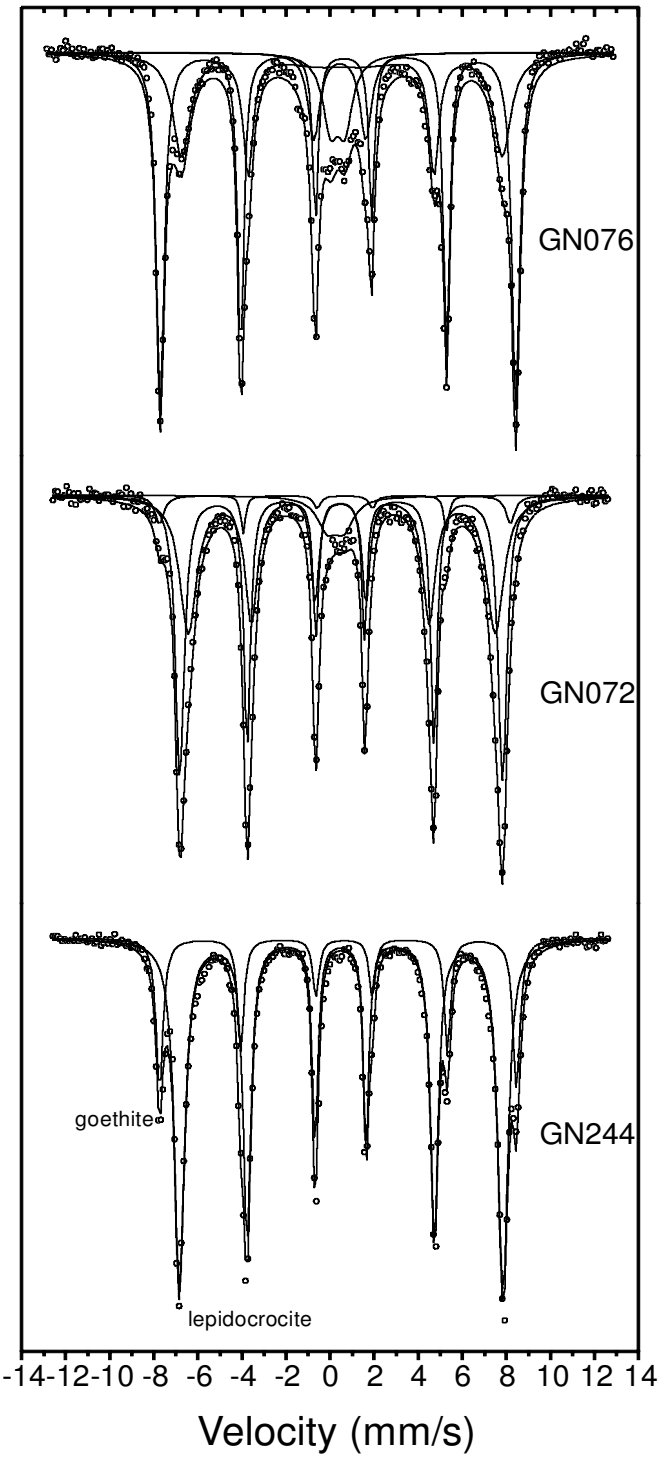

Figure 2. Mössbauer spectra of samples GN244, GN072 and GN076 from Atlantis and Thetis Deeps, at 5 K. Experimental points and fit are shown. The lepidocrocite in GN072 was fitted using two sextets.

0.55 ± 0.02 mm s^{-1} and isomer shifts of 0.37 ± 0.02 mm s^{-1}. In addition, a minor Fe^{2+} doublet with a quadrupole splitting of 2.32 ± 0.02 mm s^{-1}, an isomer shift of 1.06 ± 0.02 mm s^{-1}, and a relative area of 5% was found in the spectrum of sample GN072. In the room-temperature spectrum of sample GN076, both the ferrous doublet (~10%) and the broadlined sextet due to goethite were also detected.

https://doi.org/10.1346/000986002760832784 Published online by Cambridge University Press

At 80 K, magnetic ordering takes place in part or all of the sample, as evidenced by the appearance of a sextet pattern in the spectra (not shown). The hyperfine parameters of this sextet (magnetic hyperfine field of 48.4 ± 0.3 T, quadrupole shift of -0.12 ± 0.02 mm s^{-1}, and isomer shift of 0.47 ± 0.02 mm s^{-1}) show that they are due to goethite in all samples.

At 5 K (Figure 2), the Fe^{2+} doublet in sample GN072 is not observed. This may be explained by magnetic ordering of the component. However, due to its low intensity, this component only reveals itself close to zero velocity. Likewise, a major part of the Fe^{2+} doublet in the room-temperature spectrum of sample GN076 disappears at 5 K. However, due to the presence of clay minerals, parts of both the ferrous and the ferric doublets remain paramagnetic at this temperature. In the 5 K spectrum of sample GN076 (Figure 2) a major part of the Fe^{2+} component is very strongly overlapped by the dominant ferric sextets due to lepidocrocite and goethite. The Fe^{2+} component exhibiting magnetic order is probably due to a Mn-siderite phase, as also indicated by XRD (Table 2).

The spectrum of sample GN244 measured at 5 K exhibits two clearly-resolved sextets (Figure 2). The sextet having the highest hyperfine field is due to goethite and will not be considered further here. The 5 K spectrum of sample GN076 also revealed two clearly-resolved sextets due to goethite and lepidocrocite. The additional paramagnetic components in the spectra were fitted using doublets. The spectrum of sample GN072 at 5 K is dominated by an asymmetric sextet and a sextet pattern due to goethite can just be discerned. The application of one sextet only for the asymmetric component does not produce a very good fit, but suffices to demonstrate that it is due to lepidocrocite.

A possible clue to the origin of the difference between the samples was obtained by studying the samples between 5 K and the ordering temperature (not shown). A modest rise in temperature induced the appearance of a very broadlined component in the spectrum of sample GN072, whereas the spectrum of sample GN244 remains symmetrical in shape. Considering the polydispersity of this sample, as shown by XRD, two sextets were introduced to fit the lepidocrocite component in the Mössbauer spectrum. This improved the fit considerably (Figure 2) as would be expected from the arbitrary addition of more sextets. In the present case, however, two independent findings support the use of two sextets. The magnetic hyperfine field of one of the sextets is reduced relative to pure lepidocrocite (Table 3). The relative area of the two sextets is close to unity, which is different from the ratio of the two components as estimated from XRD. Because the analyses of XRD data suggested that both populations of crystals were free of substitutions, it is suggested that the observed reduction of the hyperfine field is essentially due to small size effects only (possibly combined with changes in anisotropy constant as Si is absorbed (see below)). A size distribution may also contribute to the high line-width found in sample GN076, but because of the dominant goethite content, a more detailed study is not possible.

Using the relative spectral area of the fits of the spectra measured at 5 K, lepidocrocite comprises ~95% (GN072), 32% (GN076) and 100% (GN244) of the Fe in the samples, in reasonable agreement with the XRD results. The hyperfine parameters at 5 K of the lepidocrocite are compared in Table 3. It is concluded that the lepidocrocites in the samples are markedly different in properties, sample GN244 having the characteristics of a more crystalline structure and relatively large crystals, *i.e.* the magnetic hyperfine field is higher and the lines are sharper.

The hyperfine field determined for sample GN244 (45.5T) is close to the maximum value reported in the literature (45.8 T) (Cornell and Schwertmann, 1996), indicating a high purity. On the other hand, samples GN076 and GN072 (in particular) exhibit a range of crystal sizes. Thus the differences in the spectra can be explained on size-dependent effects and no substitution in the structure was detected.

High-resolution transmission electron microscopy

Morphology. Two different morphologies were observed in the GN072 sample: subhedral plates in the 15–120 nm range (Figure 3a), and elongated crystals 4 nm wide and up to 100 nm long. An angle of nearly 90° between neighboring crystal faces was observed (Figure 3b). On elongate crystals only the (010) faces were well developed. In sample GN076, subhedral elongate crystals

Table 3. Hyperfine parameters of lepidocrocite from Atlantis II (GN072, GN076) and Thetis Deeps (GN244) at 5 K.

Sample	B_{hf} (T)	Isomer shift (mm/s)	Quadrupole shift (mm/s)	FWHM[1] (mm/s)
GN072 one sextet	44.9 ± 0.2	0.49 ± 0.02	0.02 ± 0.02	0.78 ± 0.02
GN072	45.4 ± 0.2	0.49 ± 0.02	0.01 ± 0.02	0.48 ± 0.03
Two sextets	43.2 ± 0.2	0.50 ± 0.02	0.03 ± 0.02	0.82 ± 0.03
GN076	45.1 ± 0.2	0.52 ± 0.02	0.02 ± 0.02	0.96 ± 0.05
GN244	45.5 ± 0.2	0.50 ± 0.02	0.01 ± 0.02	0.55 ± 0.03

[1] FWHM: Full width at half maximum of lines 1 and 6

https://doi.org/10.1346/000986002760832784 Published online by Cambridge University Press

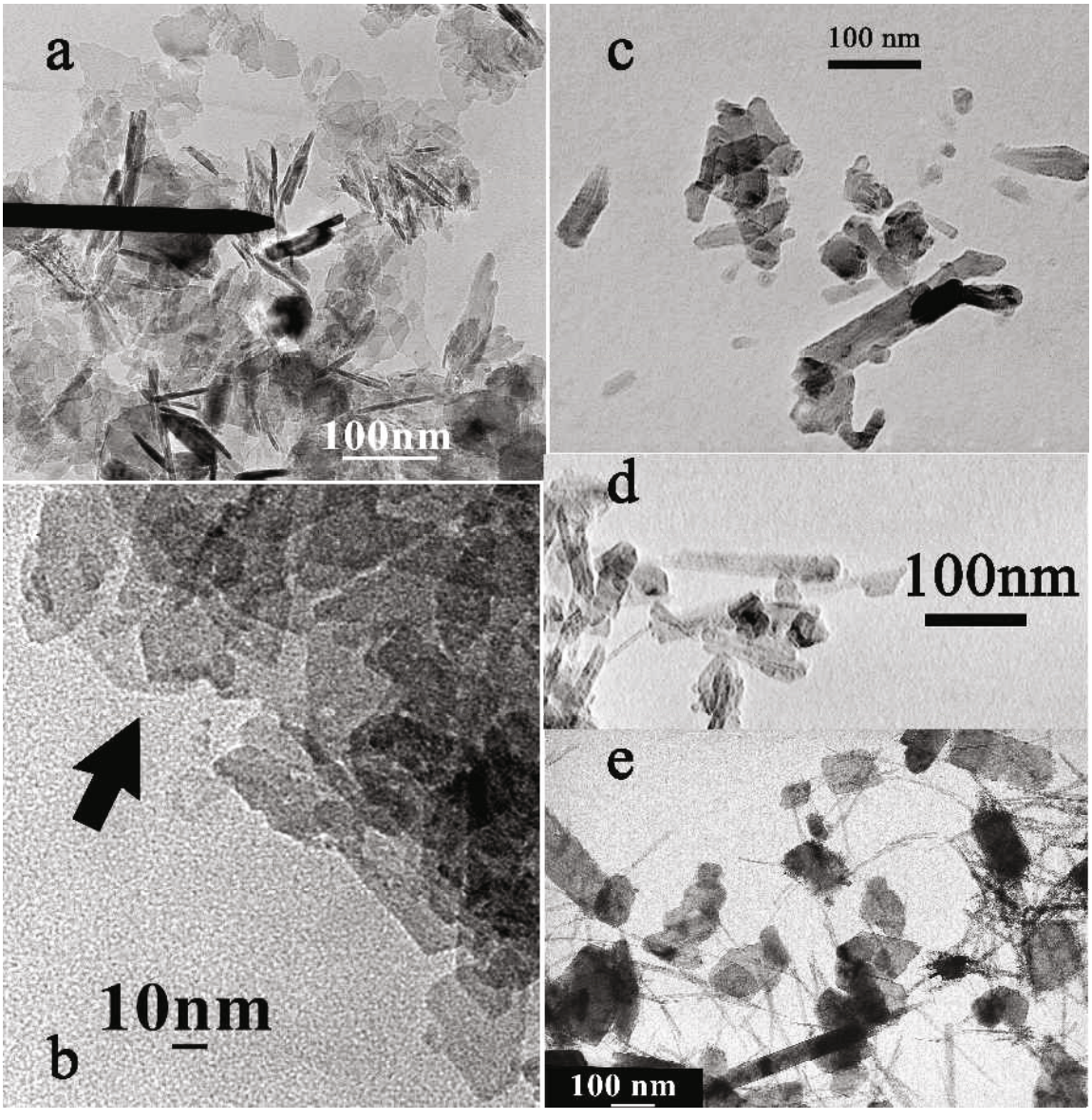

Figure 3. (a) TEM showing platy and acicular crystals of lepidocrocite from sample GN072 (arrow points at the area of chemical analysis). (b) TEM showing platy lepidocrocite from sample GN072 (arrow points at 90° between neighboring crystal faces). (c) TEM showing platy and elongate crystals of lepidocrocite from sample GN076. (d) TEM showing euhedral platy crystals of lepidocrocite from sample GN076 along with goethite. (e) TEM showing platy and acicular crystals of lepidocrocite from sample GN244.

(>100 nm) (Figure 3c) and euhedral (50 nm) plates along with goethite crystals were observed (Figure 3c,d). Euhedral plates and acicular crystals were found in sample GN244. The plates are up to 340 nm long and 140 nm wide, whereas the acicular crystals are longer (500–600 nm) and are only a few nm wide (Figure 3e). The (010) faces are well developed and the crystals commonly terminate by well-developed (101) faces.

Some of the crystals in sample GN072 lie on the [010] plane and exhibit lattice images of the 020 spacing of 0.63–0.67 nm (Figure 4a,b,c). In rod-shaped crystals only 5–6 layers were observed whereas ~40 unit layers were counted in platy crystals. It appears that the crystals are perfect with no noticeable defects. In other particles, lattice images of [120] with spacing of 0.33 nm was observed as well.

In sample GN244, platy crystals of ~40 unit layers are present with lattice images at a spacing of 0.62 nm, corresponding to *d*(020) and other crystals with a grid created by [020] fringes, with spacing at 0.619 nm and [120] fringes with spacing of 0.329 nm forming an angle of 123° (Figure 4d,e).

https://doi.org/10.1346/000986002760832784 Published online by Cambridge University Press

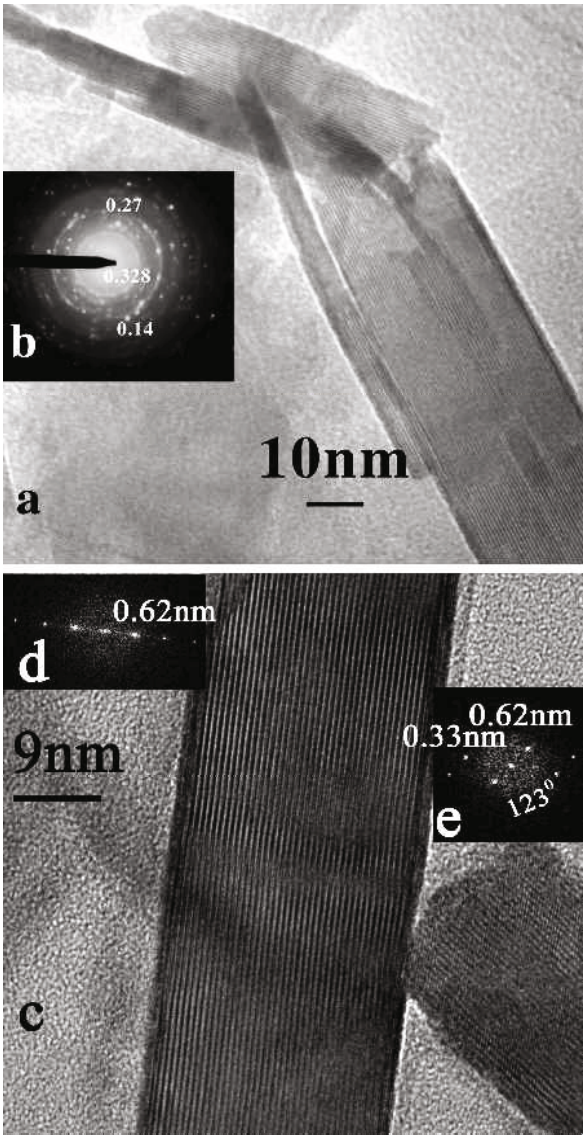

Figure 4. (a) HRTEM showing platy lepidocrocite from sample GN072. (b) Electron diffraction pattern of the particle. (c) HRTEM showing platy lepidocrocite from sample GN244. (d) Calculated (fast Fourier transformation) electron diffraction of the particle to the left. (e) Calculated (fast Fourier transformation) electron diffraction of the particle to the right.

The identification of lepidocrocite by HRTEM was confirmed by electron diffraction in which the following results were obtained for sample GN072: 0.328 nm, 0.272 nm, 0.208 nm and 0.142 nm for *hkl* 120, 011, 131 and 260, respectively (Figure 4b).

The Si/Fe mole ratios of individual crystals and of clusters of crystals from samples GN244 and GN072 are presented in Table 4. Silicon was the only foreign element associated with the lepidocrocites. The Si/Fe ratio in GN244 is close to the detection limit. In contrast, the GN072 lepidocrocite has high average Si/Fe molar ratio, in both rods and lath crystals: 0.12 ± 0.03 and 0.11 ± 0.03, respectively. Some variation in the molar ratio is noticed but generally the values are within 50% of the mean.

The results indicate that the presence of morphologies other than plates could be associated with the higher Si/Fe ratio in sample GN072. The single-plate lepidocrocite crystals in sample GN072 have on average, a Si/Fe ratio ~3 times greater than the average plate in sample GN244. As the crystalline size of sample GN072 is also smaller this could in part be explained by surface complexation only.

Differential dissolution and chemical analyses

Most of the samples were dissolved by oxalate and DCB and the results of elemental analyses of the extracts are summarized in Table 5. The relative oxalate dissolution reflects the content of other Fe-containing phases, being less reactive than lepidocrocite. The Zn and Cu concentrations in all samples are very low and are not reported in the Table. This finding is contrary to earlier studies (Scholten *et al.,* 1991). Chemical analyses of the extracts from various treatments and chemical analyses performed directly on some crystals with EDX consistently show that the only element associated with Fe in the lepidocrocite is Si. The concentration of Si in GN072 is significantly higher than in GN244. The Si/Fe ratios obtained from EDX analyses are slightly higher as compared to values obtained from analyses of the extracts. The reason for this deviation is not known in detail, but it is suggested that polymerization of the Si (see below) may have an influence on the analysis of Si by ICP.

Infrared spectroscopy

Absorbance and reflectance IR spectra are presented in Figure 5 and Table 6. In the OH-stretching region, the peak of the νOH $B_{2u(y)}$OH vibrations (GN072 = 3142 cm^{-1} and GN244 = 3128 cm^{-1}) lie between 3160 cm^{-1}, which is attributed to plate morphology, and 3060 cm^{-1}, which is attributed to rod morphology of lepidocrocite (Lewis and Farmer, 1986). This is in good agreement with the occurrence of both morphologies as observed by TEM. The band position shifts towards higher wavenumbers in GN076 due to mixture with goethite. In all samples, δOH $B_{2u(y)}$ in-plane bending at 1157–1168 cm^{-1} and δOH $B_{3u(x)}$ in-plane bending at 1020–1025 cm^{-1} were detected (Lewis and Farmer, 1986). The δOH $B_{2u(y)}$ in-plane bending and δOH $B_{3u(x)}$ in-plane bending have narrower peaks in the absorbance mode in sample GN244 indicating better crystallinity in this sample.

The γOH bending out of plane was noticed in sample GN072 and GN244 at 744–5 cm^{-1}. It was suggested that increase in the νOH-stretching frequency and decrease of γOH bending out-of-plane frequency correlate with weakening of the H bonds, due to loss of

https://doi.org/10.1346/000986002760832784 Published online by Cambridge University Press

Table 4. The Si/Fe molar ratios of lepidocrocite from Atlantis II and Thetis Deeps from point analyses in analytical TEM.

		GN072		GN244	
Morphology	Si/Fe	Morphology	Si/Fe	Morphology	Si/Fe
Cluster of rods	0.1109	Single plate	0.1036	Single plate	0.075
Few rods	0.1159	Single plate	0.1418	Single plate	0.037
Cluster of rods	0.1666	Single plate	0.0699	Single plate	0.061
Single rod	0.1500	Single plate	0.1472	Single plate	0.026
Single rod	0.0885	Single plate	0.0645	Single plate	0.005
		Single plate	0.1039	Single particle	0
		Plate between rods	0.1311	Single particle	0.026
		Plate between rods	0.1085		
Average rods	0.1264 ± 0.03	Average plates	0.1088 ± 0.03		
Average all particles		0.1156 ± 0.03		Average all particles	0.033 ± 0.027

crystallinity, caused by substitution of Fe by Al (Schwertmann and Wolska, 1990). Such an effect was not noticed in the present samples, in agreement with the absence of Al in the samples.

The $\tau O\ B_{2u(y)}$ displacement of O^{2-}(525 cm^{-1}) and $\tau O\ B_{1u(z)}$ displacement of O^{2-} (474 cm^{-1}) appear as separate vibrations in sample GN244, whereas they merge into a single, intensified band in sample GN072 at 474 cm^{-1} (Figure 5), indicating poorer crystallinity (Lewis and Farmer, 1986). The relatively high content of goethite in sample GN076 prevents this from being observed.

Peak fitting of the IR spectra indicated that in addition to lepidocrocite, two extra vibrations appear at 1049–1104 cm^{-1} and at 974–998 cm^{-1}. It is suggested that both peaks be attributed to Si–O-stretching vibrations. The band at 974–998 cm^{-1} is similar to the band found in ferrihydrite that contains ~4% Si (Schwertmann and Thalmann, 1976) and is attributed to a Si–O-stretching vibration, which is influenced by the presence of neighboring Fe ions, whereas the band at 1049–1104 cm^{-1} is probably due to a Si–O-stretching vibration, which is less affected by Fe, and has values close to those of silica gel (1080 cm^{-1}) (Schwertmann and Thalmann, 1976). Comparison between the absorbance and reflectance spectra can be used to differentiate between adsorption and substitution. It appears that both Si–O peak areas are significantly intensified in the reflectance spectra. If Si–O forms a monolayer on the lepidocrocite surface, the reflected 974–998 cm^{-1} band should be enhanced, because it is close to an Fe ion. If more than one Si–O layer is adsorbed on the surface, then the reflectance at 1049–1104 cm^{-1} should be enhanced. The presence of a separate SiO_2 phase is excluded because it would have appeared in the absorbance spectra. Therefore it is suggested that Si, which is adsorbed on the surface, forms either more than one layer, or clusters of Si–O. Two absorption bands due to goethite at 892 and 795 cm^{-1} (Cambier, 1986) are noticed in GN244 and GN076. A vibration of Mn-siderite at 871 cm^{-1} was noticed in samples GN076 and GN072.

Formation process

Bischoff (1969) suggested that precipitation of Fe^{3+} oxides occurs within the upper brine where dissolved Fe^{2+} is oxidized by O_2 diffusing from the overlying Red Sea Deep Water and transforms later into goethite and hematite. This model left lepidocrocite precipitation unexplained. Lepidocrocite occurs in the A2D either in the lowermost Detrital-Oxidic-Pyritic (DOP) Zone as finely laminated sediments with goethite, or at the lower part of the newly-formed amorphous-silicate (AM Zone) as a thin, widespread, monomineralic layer. It has been suggested (Schwertmann and Taylor, 1979), that lepidocrocite forms from oxidation of Fe^{2+} and an increased oxidation rate of Fe^{2+} favors lepidocrocite over goethite crystallization (Cornell and Schwertmann, 1996). Similar formation conditions might have occurred during lepidocrocite crystallization in the DOP zone in the A2D. The almost NaCl-saturated hot fluids, enriched

Table 5. Fe and Si/Fe ratios in oxalate and DCB extracts in samples from Atlantis II and Thetis Deeps.

Sample	Si/Fe (molar) in oxalate extracts	% Dissolved as FeOOH (oxalate)	Si/Fe (molar) in DCB extracts	% Dissolved as FeOOH (DCB)
GN072	0.058	82	0.089	94
GN076	0.048	42	0.03	n.d.
GN244	0.011	100	0.012	n.d.

n.d.: not determined

https://doi.org/10.1346/000986002760832784 Published online by Cambridge University Press

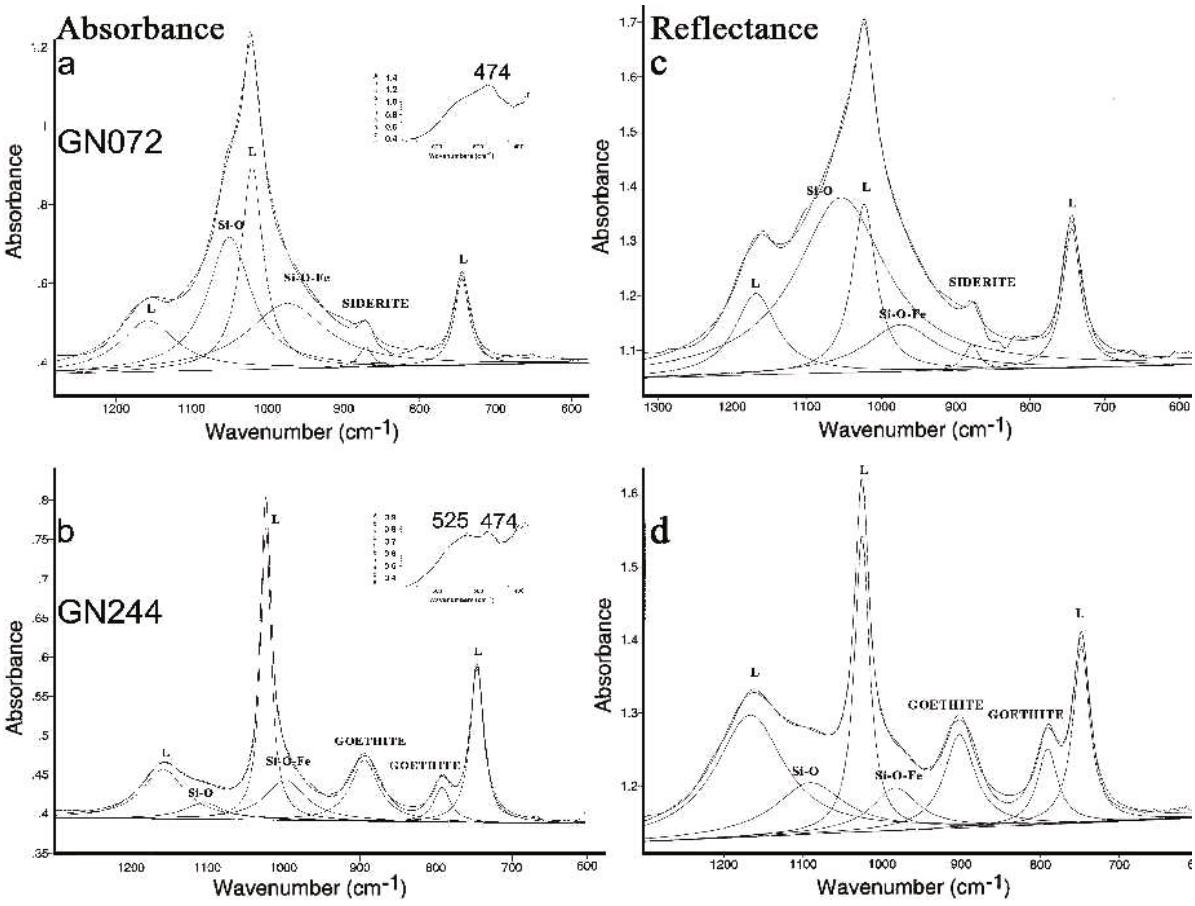

Figure 5. (a) FTIR absorbance spectra of GN072 (400–590 cm range in the inset section). (b) FTIR absorbance spectra of GN244 (400–590 cm^{-1} range in the inset section). (c) FTIR reflectance spectra of GN072. (d) FTIR reflectance spectra of GN244.

with Fe and Si, which originated from the interaction with sediments (Dupré *et al.,* 1988) and the basalt underneath (Anschutz *et al.,* 1995) discharged into the Atlantis II Deep, creating only local pools (Shanks and Bischoff, 1980). Since Fe^{2+} is common in the DOP Zone in A2D in the form of pyrite or Mn-siderite, it might have dissolved and served as a precursor for lepidocrocite formation. A relatively rapid mixing of these fluids with oxidized Red Sea Deep Water led to lepidocrocite crystallization.

In TD, the almost mono-mineralic lepidocrocite was found in Fe-facies in the upper part of the sediments. This widespread lepidocrocite crystallized during rapid Fe^{2+} oxidizing conditions, while hot brines filled the deep and a wide mixing layer was probably formed. A large amount of dissolved oxygen was probably introduced into the upper part of the brine by oxidized dense brine initially formed in the northern part of the Red Sea. The abrupt down welling of the oxidized water was followed by rapid precipitation of lepidocrocite in TD.

Table 6. Peak positions and area from IR spectra (absorbance and DRIFT).

Sample		δOH B_{2u}[1]	Area[2]	Width	Si–O[1]	Area[2]	δOH B_{2u}[1]	Area[2]	Width	Si–O–Fe[1]	Area[2]	Sum area[2]
GN072	absorbance	1157	16	90	1049	34	1020	27	35	974	29	106
	reflectance	1168	14	67	1054	63	1023	18	39	974	13	108
GN076[3]	absorbance	1162	1	46	1051	21	1021	20	53	999	30	72
GN244	absorbance	1158	6	68	1104	2	1023	10	17	998	5	23
	reflectance	1167	23	104	1091	10	1025	14	23	983	6	53

[1] wavenumber measured in cm^{-1}
[2] area measured in arbitrary units
[3] This sample contains more goethite than lepidocrocite

https://doi.org/10.1346/000986002760832784 Published online by Cambridge University Press

The size and morphology of the lepidocrocite is possibly related to Si concentration within the brine. Karim and Newman (1986) noticed that soil lepidocrocite precipitation was hindered at elevated Si concentration. Similar effects were noticed in the crystallization of lepidocrocite from solutions with varying Si/Fe ratios (Schwertmann and Thalmann, 1976).

It is suggested that high Si concentrations might have hindered crystal growth and led to smaller and less crystalline lepidocrocite in the A2D, whereas lower initial Si concentrations in the TD led to larger and more crystalline lepidocrocite. Bimodal distribution of crystal size in GN072 can be explained by a short-term reduced Si concentration in the discharging fluids leading to crystallization of larger crystals. Such fluctuations in hydrothermal activity, which have been common during the last few decades (Hartmann *et al*., 1998a,b), probably happened also during the precipitation of DOP zone. Different settling velocities related to crystalline size might have created bimodal distribution of crystal size in the sediments (GN072).

Taylor (1984) suggested that an elevated [Cl]/[Fe] ratio in the initial solution was found to influence the oxidation rate during lepidocrocite formation and increasing [Cl] initially induced a greater degree of lepidocrocite crystallinity. Precipitation of lepidocrocite in both deeps probably occurred in the mixing zone between the Red Sea Deep Water and the underlying condensed, hydrothermal brine. In both deeps, the confining environments, during lepidocrocite precipitation, were almost pure NaCl solutions and the initial [Cl]/[Fe] ratios were at least 100 fold greater than the experimental conditions described by Taylor (1984). Combining these data with Si restriction of crystal growth, we can assume that in TD, Si restriction of crystal growth was less effective and the high crystallinity was achieved due to an elevated [Cl]/[Fe] ratio contrary to the A2D, where [Si] concentration was greater, restriction of crystal growth was more effective, leading to lower crystallinity of the GN072 and GN076 samples.

CONCLUSIONS

Lepidocrocite from Red Sea hydrothermal deposits appears in the form of small subhedral to euhedral crystals ranging in size from 4×100 nm in the A2D, up to 340×140 nm in the TD. Two forms of crystals were observed: plates and elongate rods. Although the samples were crystallized in hydrothermal brines which are enriched in Pb, Cu, Mn and Zn (Craig, 1969) with respect to seawater, it appears that only Si is associated with Fe in the lepidocrocite. The Si/Fe (molar) ratio reaches 0.11 in the A2D samples and does not appear to affect the perfect lattice image fringe along [010]. The TEM demonstrates different morphologies of the crystals. X-ray diffraction, Mössbauer spectroscopy and IR spectra indicate that the A2D lepidocrocite is less crystalline than the TD lepidocrocite, which has a distinctly lower Si/Fe molar ratio (0.03). It appears that Si is not incorporated into the crystal but adsorbed on the surface mostly as monomers but also forming polymers.

The formation of A2D lepidocrocite is probably due to rapid oxidation of Fe^{2+} in Si-rich brine, whereas the TD lepidocrocite crystallized from Si-poor brine.

ACKNOWLEDGMENTS

Prof. P. Stoffers, Institute for Geosciences, University of Kiel, Germany is thanked for supplying the samples. We are also grateful to Mr D. Magelanski from Ben-Gurion University, Beer Sheva, Mr A. Henschel from the Technical University of Denmark Lyngby and Mr V. Ezersky from Ben-Gurion University, Beer Sheva, for their technical assistance with XRD and HRTEM analyses; and to Miss Krongauz and Dr Shoval from the Open University of Israel, Tel Aviv and Dr Chertkova from the Hebrew University, Rehovot, Israel for their assistance with the IR analyses. Dr Scholten, Dr Stanjek and an anonymous reviewer are acknowledged for their helpful and constructive comments on the manuscript.

REFERENCES

Anschutz, P., Blanc, G. and Stille, P. (1995) Origin of fluids and the evolution of the Atlantis II deep hydrothermal system, Red Sea: strontium isotope study. *Geochimica et Cosmochimica Acta,* **59**, 4799–4808.

Bäcker, V.H. and Richter, H. (1973) Die rezente hydrothermal-sedimentäre Lagerstätte Atlantis. II. Tief im Roten Meer. *Geologische Rundschau,* **62**, 697–737.

Bignell, R.D. (1975) The geochemistry of metalliferous brine precipitates and other sediments from the Red Sea. Unpublished Ph.D. thesis, University of London, London, 276 pp.

Bischoff, J.L. (1969) Red Sea geothermal brine deposits: their mineralogy, chemistry and genesis. Pp. 368–401 in: *Hot Brines and Recent Heavy Metal Deposits in the Red Sea* (E.T. Degens and D.A. Ross, editors). Springer-Verlag Berlin/Heidelberg/ New York.

Butuzova, G.Yu. and Lisitsyna, N.A. (1984) Metal deposits in deep subbasins of the Red Sea; ore geochemistry and distribution pattern. *Lithology and Mineral Resources USSR,* **18**, 224–238.

Butuzova, G.Yu., Dritz, V.A., Morozov, A.A. and Gorschkov, A.I. (1990) Processes of formation of iron-manganese oxyhydroxides in Atlantis II and Thetis Deeps in the Red Sea. *Special Publications of the International Association of Sedimentology,* **11**, 57–72.

Cambier, P. (1986) Infrared study of goethite of varying crystallinity and particle size. I. Interpretation of OH and lattice vibration frequencies. *Clay Minerals,* **21**, 191–200.

Cornell, R.M. and Schwertmann, U. (1996) *The Iron Oxides, Structure, Properties, Reactions, Occurrence and Uses.* VCH Verlagsgesellschaft GmbH Weinheim, New York 573 pp.

Craig, H. (1969) Geochemistry and origin of the Red Sea brines. Pp. 208–242 in: *Hot Brines and Recent Heavy Metal Deposits in the Red Sea* (E.T. Degens and D.A. Ross, editors). Springer-Verlag Berlin/Heidelberg/New York,.

Danielsson, L.G., Dyrssen, D. and Graneli, A. (1980) Chemical investigation of Atlantis II and discovery brines in the Red Sea. *Geochimica et Cosmochimica Acta,* **44**, 2051–2065.

Dupré, B., Blanc, G., Bolegue, J. and Allegre, C.J. (1988) Metal remobilization at a spreading centre studied using lead isotopes. *Nature,* **333**, 165–167.

Hartmann, M., Scholten, J.C., Stoffers, P. and Wehner, F. (1998a) Hydrographic structure of brine filled deeps in the Red Sea – new results from Shaban, Kerbit, Atlantis II and Discovery Deep. *Marine Geology*, **144**, 311–330.

Hartmann, M., Scholten, J.C. and Stoffers, P. (1998b) Hydrographic structure of brine filled deeps in the Red Sea: Correction of Atlantis II Deep temperatures. *Marine Geology,* **144**, 331–332.

Karim, Z. and Newman, A.C.D. (1986) The possible effect of soluble silicon on the lepidocrocite content of gley soils from England and Bangladesh. *Journal of Soil Science,* **37**, 259–266.

Lewis, D.G. and Farmer, V.C. (1986) Infrared absorption of surface hydroxyl groups and lattice vibrations in lepidocrocite (γ-FeOOH) and boehmite (γ-AlOOH). *Clay Minerals,* **21**, 93–100.

McKeague, J.A. and Day, J.H. (1966) Dithionite- and oxalate-extractable Fe and Al as aids in differentiating various classes of soils. *Canadian Journal of Soil Science,* **46**, 13–22.

Mehra, O.P. and Jackson, M.L. (1960) Iron oxides removal from soils and clays by dithionite-citrate system buffered with sodium bicarbonate Pp. 317–327 in: *Proceedings of the 7th National Conference of the Clay Minerals Society, Washington, D.C.*, 1958 (A. Swineford, editor). Pergamon Press, New York.

Niemeyer, J., Chen, Y. and Bollag, J.M. (1992) Characterization of humic acids, composts and peat by diffuse reflectance Fourier Transform infrared spectroscopy. *Soil Science Society of America Journal,* **56**, 135–140.

Schoel, M. and Faber, E. (1978) New isotopic evidence for the origin of Red Sea brines. *Nature,* **275**, 436–438.

Scholten, J.C. (1984) Mineralogische Untersuchungen an Sedimentkernen aus dem Thetis-Tief, Rotes Meer. Thesis, Universität Heidelberg, Heidelberg, Germany, 53 pp.

Scholten, J.C., Stoffers, P., Walter, P. and Plunger, W. (1991) Evidence for episodic hydrothermal activity in the Red Sea, from the composition and formation of hydrothermal sediments, Thetis Deep. *Tectonophysics,* **190**, 109–117

Schwertmann, U. (1959) Die fraktionierte Extraktion der freien Eiseoxyde in Boden, ihre mineralogischen Formen und ihre Entstehungsweisen. *Zeitschrift für Pflanzenernährung Düngung und Bodenkunde,* **84**, 194–204.

Schwertmann, U. (1964) Differenzierung der Eisenoxide des Bodens durch Extraktion mit Ammoniumoxalat-Lösung. *Zeitschrift für Pflanzenernährung Düngung und Bodenkunde*, **105**, 194–202.

Schwertmann, U. and Taylor, R.M. (1979) Natural and synthetic poorly crystallized lepidocrocite. *Clay Minerals,* **14**, 285–293.

Schwertmann, U. and Thalmann, H. (1976) The influence of [Fe(II)], [Si] and pH on the formation of lepidocrocite and ferrihydrite during oxidation of aqueous $FeCl_2$ solutions. *Clay Minerals,* **11**, 189–200.

Schwertmann, U. and Wolska, E. (1990) The influence of aluminum on iron oxides, XV. Al-for-Fe substitution in synthetic lepidocrocite. *Clays and Clay Minerals,* **38**, 209–212.

Schwertmann, U., Friedl, J., Stanjek, H., Murad, E. and Bender Koch, C. (1998) Iron oxides and smectites from the Atlantis II Deep, Red Sea. *European Journal of Mineralogy,* **10**, 953–967.

Shanks III, W.C. and Bischoff, J.L. (1980) Geochemistry, sulfur isotope composition, and accumulation rates of Red Sea Geothermal deposits. *Economic Geology and the Bulletin of the Society of Economic Geologists,* **75**, 445–459.

Stoffers, P. and Ross, D.A. (1972) Sedimentary history of the Red Sea. Pp. 849–865 in: *Initial Report of the Deep Sea Drilling project* **XXIII** (P.R Supko and O.E. Weser, editors).

Taylor, R.M. (1984) Influence of chloride on the formation of iron oxides from Fe(II) chloride. II. Effect of [Cl] on the formation of lepidocrocite and its crystallinity. *Clays and Clay Minerals,* **32**, 173–180.

(*Received 1 September 2000; revised 28 August 2001; Ms. 485; A.E. Helge Stanjek*)